Polarization-engineered GaN/InGaN/GaN tunnel diodes

Sriram Krishnamoorthy,[a] Digbijoy N. Nath, Fatih Akyol, Pil Sung Park, Michele Esposto, and Siddharth Rajan
Department of Electrical and Computer Engineering, The Ohio State University, Columbus, Ohio 43210, USA

(Received 19 August 2010; accepted 25 October 2010; published online 16 November 2010)

We report on the design and demonstration of polarization-engineered GaN/InGaN/GaN tunnel junction diodes with high current density and low tunneling turn-on voltage. Wentzel–Kramers–Brillouin calculations were used to model and design tunnel junctions with narrow band gap InGaN-based barrier layers. N-polar p-GaN/$In_{0.33}Ga_{0.67}N$/n-GaN heterostructure tunnel diodes were grown using molecular beam epitaxy. Efficient interband tunneling was achieved close to zero bias with a high current density of 118 A/cm^2 at a reverse bias of 1 V, reaching a maximum current density up to 9.2 kA/cm^2. These results represent the highest current density reported in III-nitride tunnel junctions and demonstrate the potential of III-nitride tunnel devices for a broad range of optoelectronic and electronic applications. © *2010 American Institute of Physics*.
[doi:10.1063/1.3517481]

The phenomenon of interband tunneling across degenerately doped p-n junction, reported by Esaki,[1] has been exploited in a variety of device applications such as light emitting diodes (LEDs), laser diodes, multijunction solar cells,[2,3] and more recently, tunnel field effect transistors (TFETs).[4] Tunnel junctions enable multiple active region emitters and multijunction solar cells due to their low resistance in reverse and forward bias regimes, respectively. In wide band gap devices such as III-nitride lasers and LEDs,[5,6] efficient tunnel junctions (TJs) may mitigate losses due to high resistance p-type layers and p-contacts. Tunneling based devices such as the TFETs are also promising for high performance and low-power computation as they offer a way to achieve subthreshold swing below the 60 mV/decade limit.

Extensive research has led to efficient interband tunneling based devices in material systems such as the III-As and SiGe.[7] While degenerately doped p-n tunnel junctions have been used to replace resistive p-GaN with n-GaN as the top contact layer for LED structures,[8,9] the III-nitride material system still lacks an efficient tunnel junction due to the large band gap and dopant solubility limits. For example, even with a very high doping of 10^{20} cm^{-3}, the depletion width of a standard p+/n+ GaN junction is 6 nm, but the large potential barrier due to higher band gap leads to high tunneling resistance and low current density.

The high spontaneous and piezoelectric polarization charge[10] along the c-axis of III-nitrides and other highly polar semiconductors provides a new design approach for tunneling structures. In a conventional tunnel junction, the degenerate doping reduces the space charge region thickness and creates band bending at the junction to align the valence and conduction bands on either side of the space charge region. The space charge dipole created by ionized donors and acceptors can be substituted with the fixed positive and negative polarization sheet charges at polar heterointerfaces. In heterostructures of highly polar materials such as nitrides, polarization induced dipole can create significantly high electric fields resulting in large band bending over a small distance, thereby increasing the tunneling probability. This principle of polarization induced tunnel junction[11,12] was demonstrated using AlN as the barrier material for interband tunneling in GaN. However, the large band gap of AlN reduces tunneling probability and the GaN/AlN/GaN devices have low current density and high tunneling resistance.

Tunneling probability across a potential barrier is determined by the barrier height and the thickness of the barrier material. Hence, it is expected that for the same tunneling width, a lower band gap material will be a more efficient tunnel barrier between wide band gap materials. It may therefore be expected that $In_xGa_{1-x}N$ with its low band gap and a large piezoelectrically induced polarization when coherently strained to GaN is an ideal candidate for efficient interband tunneling. In this Letter, we investigate the potential of InGaN as a barrier material for efficient interband tunneling in GaN through calculations based on polarization and Wentzel–Kramers–Brillouin (WKB) approximation. We also demonstrate an InGaN-based tunnel junction grown by plasma assisted molecular beam epitaxy (PAMBE) with very high current density surpassing previous doping and GaN/AlN/GaN based tunnel diodes.

The equilibrium band diagram of the proposed GaN/InGaN/GaN tunnel junction is shown in Fig. 1. For interband tunneling to occur at a very low reverse bias, the InGaN composition and thickness are chosen such that the polarization induced band bending aligns the conduction and valence band on either side of the sandwiched InGaN layer. GaN is degenerately doped to reduce the depletion region thickness at the GaN/InGaN interface, and hence the major barrier to tunneling is the InGaN layer. Under reverse bias, the electrons in the valence band of p-GaN tunnel across the p-depletion region (intravalence band), InGaN (interband), and n-depletion region (intraconduction band), entering the conduction band of n-GaN, as shown in the inset of Fig. 1. The equilibrium band bending Φ due to $In_xGa_{1-x}N$ layer of thickness "t" is $\Phi(x)=q\ \sigma(x)t/\varepsilon(x)$, where $\varepsilon(x)$ is the permittivity of $In_xGa_{1-x}N$ and $\sigma(x)$ is the fixed polarization induced charge density at the GaN/$In_xGa_{1-x}N$ interface.[13] For

[a]Author to whom correspondence should be addressed. Electronic mail: krishnas@ece.osu.edu. Tel.: +1-614-688-8458.

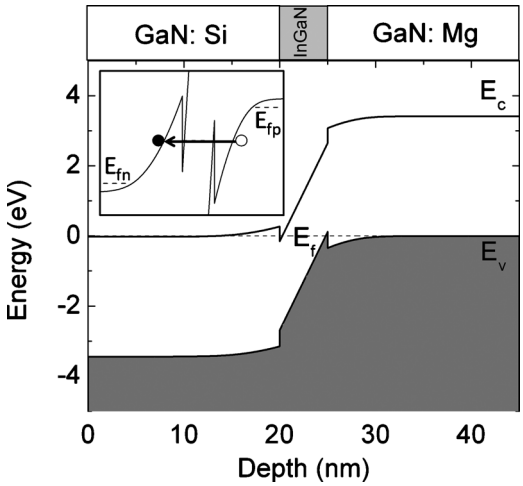

FIG. 1. Equilibrium energy band diagram of GaN/$In_{0.33}Ga_{0.67}N$/GaN zero bias interband tunnel junction. Inset: band diagram at reverse bias showing interband tunneling.

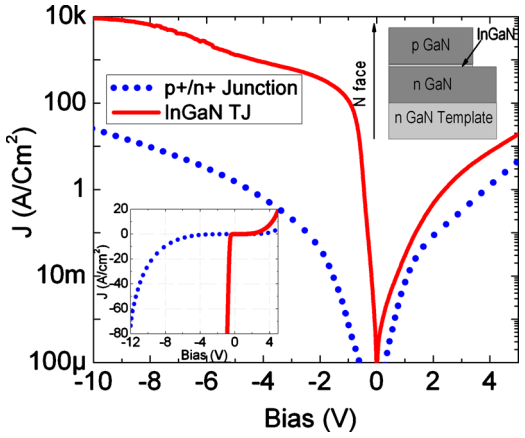

FIG. 3. (Color online) Log J-V characteristics of the GaN/$In_{0.33}Ga_{0.67}N$/GaN TJ (solid line) and standard p+/n+ junction (dotted line). Inset (top right): epitaxial structure of the InGaN TJ sample. Inset (bottom left): linear J-V characteristics of the GaN/$In_{0.33}Ga_{0.67}N$/GaN TJ (solid line) and reference p+/n+ junction (dotted line).

a critical InGaN layer thickness, t_{cr}, the equilibrium potential drop in the InGaN layer equals the band gap of the InGaN layer, $E_{g,InGaN}$. If $t < t_{cr}$, tunneling probability is very low since conduction and valence band extrema on either side are not aligned. With $t > t_{cr}$, tunneling probability reduces due to the increased thickness of the barrier. Figure 2 shows the variation of the critical thickness t_{cr} with the InN mole fraction in InGaN. The critical thickness t_{cr} decreases with increasing In composition due to the combined effects of increasing polarization charge and decreasing band gap. For the critical thickness t_{cr}, the potential barrier V (t) seen by an electron is a triangular barrier of width t_{cr} and maximum height of $E_{g,InGaN}/q$, as illustrated in the inset of Fig. 2. The tunneling probability p across the barrier for a critical thickness t_{cr} is evaluated by using WKB approximation[14] given by

$$p(t_{cr}) = \exp\left(-2\int_0^{t_{cr}} \sqrt{\frac{2m^* E_{g,InGaN} t}{\hbar^2 q t_{cr}}}\,dt\right), \quad (1)$$

where m^* is the effective mass of InGaN.

The tunneling probability "p" calculated using Eq. (1) is found to increase as the In composition in the barrier material is increased (Fig. 2). Also, the tunneling probability for a GaN/AlN(2.6nm)/GaN structure, calculated to be $\sim 10^{-11}$, is shown for comparison as a dotted line in Fig. 2. This is the optimal thickness and composition for an AlGaN-based tunnel junction. It can be observed that for higher In composition, the tunneling probability of the GaN/InGaN/GaN TJ is several orders of magnitude higher than that for GaN/AlN/GaN TJ. It should be noted that only the tunneling across the InGaN barrier is considered in calculating the probability, and this component increases as the In composition is increased. However, for very high In compositions at which the band offsets are of the order of band gap of InGaN, tunneling barrier due to the depletion regions at the GaN/InGaN heterojunctions can no longer be neglected and may play a significant role in reducing the tunneling probability.

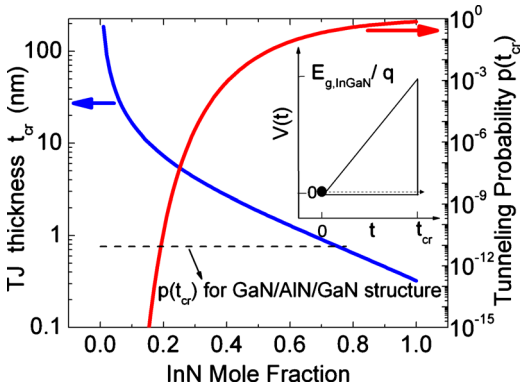

FIG. 2. (Color online) Critical tunnel junction thickness t_{cr} in order to achieve zero bias interband tunneling is shown as a function of InN mole fraction in InGaN. Tunneling probability computed as a function of InN mole fraction in InGaN for a barrier thickness of t_{cr} is shown. Dotted line indicates a tunneling probability of 10^{-11} for a GaN/AlN(2.6nm)/GaN structure. Inset: potential profile of the barrier for electron tunneling used for calculation of p.

To demonstrate the potential advantage in using a GaN/InGaN/GaN structure, an InGaN TJ sample was grown on a Lumilog[15] N-polar free standing LED quality GaN template (dislocation density of $\sim 10^8$ cm^{-2}) by PAMBE in a Veeco Gen 930 system. The epitaxial structure of the device is shown in the inset of Fig. 3. The N-polar orientation is used in this work, as higher In incorporation can be achieved at a given growth temperature compared to the conventional Ga-polar orientation.[16,17] N-polar InGaN was grown on 100 nm thick Si doped GaN ($N_D \sim 5 \times 10^{18}$ cm^{-3}) using the conditions and growth model developed earlier.[17] The growth model enables us to grow a specified thickness and composition of InGaN while taking into account the composition and temperature dependent decomposition rate. InGaN was grown at a high substrate temperature of 600 °C for superior quality. The InGaN layer was capped with 100 nm of p GaN ($N_A \sim 1 \times 10^{19}$ cm^{-3}). The thickness and composition of the InGaN layer were assessed to be 6.4 nm and 33.5%, respectively, from ω-2θ triple-axis scans (not shown here) using a Bede high resolution x-ray diffractometer, indicating good agreement with the growth model.[18] A reference p-n junction with identical doping profiles and growth conditions but without an InGaN layer was grown as a control sample. Both the samples exhibited step flow growth morphology as seen using atomic force microscopy (not shown here). Ni/Au (20/150 nm) and Ti/Au (20/100 nm) stacks were evaporated us-

ing standard optical lithography on the p-GaN and n-GaN layers, respectively.

Figure 3 shows the typical I-V characteristic of the InGaN TJ device (30×30 μm^2) and a reference pn junction. The forward bias turn-on voltage of the TJ was lower, which we attribute to the presence of a lower band gap InGaN quantum well. Due to lower turn-on voltage, the forward bias current of the InGaN TJ is higher than the reference p-n junction sample at a given voltage. In the reverse direction, the pn junction shows reverse leakage current, which is lower than the forward current. The TJ shows much higher reverse current than in the forward direction, which is a typical behavior of a backward diode. In addition, the reverse tunneling current in the TJ was several orders of magnitude higher than in the pn junction.

Two regimes were observed in the reverse I-V characteristics for the GaN/InGaN/GaN TJ. In the low reverse bias regime, a sharp increase in reverse current was observed ($\sim$70–130 mV/decade) from zero bias (inset of Fig. 3), indicating the onset of tunneling in the device. Such a low turn-on voltage would be an ideal candidate to connect devices in series, especially in the case of multiple active region emitters. At a reverse voltage of 1 V, a current density of 118 A/cm^2 was obtained. In comparison, the reference pn junction sample had very low reverse current (five orders of magnitude lower at -1 V) as expected due to the thicker barrier in the absence of polarization induced field. At higher current density levels (>100 A/cm^2), the differential resistance increased significantly. Further analysis is needed to understand the origin of this behavior, but it may be attributed partly to increased series and contact resistances and self-heating. The maximum observed current density in reverse bias, 9.2 kA/cm^2, is the highest current density reported for III-nitride tunnel diodes. Although the maximum current density value is limited due to the characterization equipment, this demonstrates the higher current carrying capability of the tunnel junction.

While the results described here on GaN/InGaN/GaN TJs demonstrate clearly the promise of this technology, further improvements in the device characteristics can be achieved by using higher composition InGaN and optimizing barrier thickness. Further sophistication in design, such as graded GaN/InGaN interfaces to eliminate abrupt depletion barriers, asymmetric junctions, and the use of quaternary alloys, may enable lower resistance and higher tunneling current. A complete theoretical understanding and modeling of the intraband and interband tunneling transport in this structure will enable a better design of these devices. In addition, band structure effects are expected to play an important role at high current density, and a more detailed calculation incorporating these may provide insight.[19] The concept of enhancing tunneling probabilities by using a narrow gap material as a tunnel barrier demonstrated here may be used as the basis for other III-nitride alloys such as AlGaN and AlN, as well as other wide band gap material systems that have significant polarization charge (such as ZnO).

In conclusion, we have demonstrated the promise of polarization engineering using narrow band gap layers as a barrier material for interband tunneling in III-nitride devices. WKB calculations were used to model and design GaN/InGaN/GaN tunnel junctions. Extremely low tunneling resistance, tunneling turn-on close to zero bias, and high reverse current density (100 A/cm^2 at -1 V, $J_{max}=9.2$ kA/cm^2) were achieved with a $GaN/In_{0.33}Ga_{0.67}N/GaN$ tunnel junction. The tunnel junction designs demonstrated here will enable the incorporation of tunnel junctions in several technologically relevant III-nitride devices such as LEDs, lasers, and solar cells, and provide a pathway to device structures such as tunnel FETs.

We would like to acknowledge the funding from ONR (Program manager: Paul Maki) and OSU Institute for Materials Research (IMR).

[1] L. Esaki, Phys. Rev. **109**, 603 (1958).
[2] R. R. King, D. C. Law, K. M. Edmondson, C. M. Fetzer, G. S. Kinsey, H. Yoon, R. A. Sherif, and N. H. Karam, Appl. Phys. Lett. **90**, 183516 (2007).
[3] D. L. Miller, J. Appl. Phys. **53**, 744 (1982).
[4] K. K. Bhuwalka, S. Sedlmaier, A. K. Ludsteck, C. Tolksdorf, J. Schulze, and I. Eisele, IEEE Trans. Electron Devices **51**, 279 (2004).
[5] S. Nakamura, M. Senoh, S. Nagahama, N. Iwasa, T. Yamada, T. Matsushita, H. Kiyoku, and Y. Sugimoto, Jpn. J. Appl. Phys., Part 2 **35**, L74 (1996).
[6] S. Nakamura, M. Senoh, N. Iwasa, and S. Nagahama, Appl. Phys. Lett. **67**, 1868 (1995).
[7] N. Jin, S. Y. Chung, A. T. Rice, P. R. Berger, R. Yu, P. E. Thompson, and R. Lake, Appl. Phys. Lett. **83**, 3308 (2003).
[8] S. R. Jeon, Y. H. Song, H. J. Jang, G. M. Yang, S. W. Hwang, and S. J. Son, Appl. Phys. Lett. **78**, 3265 (2001).
[9] T. Takeuchi, G. Hasnain, S. Corzine, M. Hueschen, Jr., R. P. Schneider, C. Kocot, M. Blomqvist, Y. Chang, D. Lefforge, M. R. Krames, L. W. Cook, and S. A. Stockman, Jpn. J. Appl. Phys., Part 2 **40**, L861 (2001).
[10] F. Bernardini, V. Fiorentini, and D. Vanderbilt, Phys. Rev. B **56**, R10024 (1997).
[11] M. J. Grundmann and U. K. Mishra, Phys. Status Solidi C **4**, 2830 (2007).
[12] J. Simon, Z. Zhang, K. Goodman, H. Xing, T. Kosel, P. Fay, and D. Jena, Phys. Rev. Lett. **103**, 026801 (2009).
[13] I. Vurgaftman and J. R. Meyer, in *Nitride Semiconductor Devices: Principles and Simulation*, edited by J. Piprek (Wiley, Weinheim, 2007), pp. 13–48.
[14] L. D. Landau and E. M. Lifshitz, *Quantum Mechanics* (Addison-Wesley, Reading, MA, 1958), p. 174.
[15] Lumilog, Vallauris, France (www.lumilog.com).
[16] K. Xu and A. Yoshikawa, Appl. Phys. Lett. **83**, 251 (2003).
[17] D. N. Nath, E. Gür, S. A. Ringel, and S. Rajan, Appl. Phys. Lett. **97**, 071903 (2010).
[18] D. N. Nath, E. Gür, S. A. Ringel, and S. Rajan (unpublished).
[19] M. F. Schubert, Phys. Rev. B **81**, 035303 (2010).